ADVANCED FUNCTIONAL MATERIALS
www.afm-journal.de

Glycera-Inspired Synergistic Interfacial Interactions for Constructing Ultrastrong Graphene-Based Nanocomposites

*Yiren Cheng, Jingsong Peng, Hanjie Xu, and Qunfeng Cheng**

The interest in bioinspired graphene-based nanocomposites (BGBNs) is rising recently due to their exceptional mechanical properties as well as high electrical conductivities. Numerous works have suggested that the synergistic interfacial design of ionic bonding (IB) co-working with other interfacial interactions effectively improves the mechanical properties of BGBNs. However, as the ions are conventionally chelated with graphene oxide (GO) nanosheets, the relatively weak and short interlayered IB may hinder the load transfer between GO nanosheets leading to poor synergistic effects. Herein, inspired by the jaw of *Glycera*, the synergistic effect is further amplified via special IB, which stiffens the organic component. Compared with the traditional IB, the metal–ligand coordinate bonding by copper ions that is used in this work and originates from *Glycera*, selectively cross-links the chitosan chains. This *Glycera*-inspired synergistic effect strategy boosts record tensile strength to an extraordinary value of 868.6 MPa, five times higher than that of the pure reduced graphene oxide film. The additional high electrical conductivity enables applications in many fields such as flexible energy devices, supercapacitors, and other electronic devices.

1. Introduction

On account of the appealing mechanical and electrical performances, bioinspired graphene-based nanocomposites (BGBNs) mimicking the natural nacre have drawn much attention during last decades,[1] especially for the augment on the tensile strength of which the highest value has reached up to 765 MPa.[2] Recently, the synergistic effect from different interfacial interactions between graphene nanosheets is demonstrated to be an exceedingly effective strategy to improve the mechanical properties of BGBNs. Lots of works have been done, revealing that the ionic bonding (IB) shows a capability to interplay with the hydrogen bonding (HB) or the covalent bonding (CB) to optimize the interfacial interactions.[3] For example, the IB could cowork with the HB, a weaker interaction, leading to a superior mechanical behavior than that via single interfacial interaction.[3a] Or cooperating with the CB, a stronger interaction, the IB could dissipate loading energy to serve as sacrificial bonding which enhances the toughness.[3b] For promoting the tensile strength, however, the IB is relatively poor for its lower bonding energy especially for the case of intercalation between the nanosheets via ions.[4] Thus, how to use the IB to promote the tensile strength of BGBNs is essential to broaden the application of BGBNs, allowing for the benefits of multifunction from IB, such as electrical conductivity,[5] self-healing,[6] adhesion,[7] etc.

In nature, the metal ions are vital for various functions in living creatures including the formation of the hard organs for the protection or predation. The jaw of *Glycera*,[8] the hardest part of this creature, is a typical example to show the effect of ions to stiffen the organic matrix.[9] In the jaw of *Glycera*, around 2.5 wt% copper ions exist in highly aligned protein matrix, chelated by the imidazole group of histidine.[10] The as-formed metal–ligand coordinate bond possess nearly half of the strength of CB,[11] and highly cross-link the protein into a continuous matrix which facilitates the load transferring and promotes the hardness.[12] Thus, this special IB formed by the copper ions only within the organic matrix by coordinate bonds should inspire new design of interfacial interactions.

Chitosan (CS) is a kind of biodegradable and easy-available material with abundant hydroxyl and amine functional groups, promising the multiple interactions between CS and GO.[13] In our previous work,[14] the nanocomposites based on graphene oxide (GO) and CS possess admirable tensile strength of 526.0 MPa due to the synergistic effect from CB and HB. The strong CB confers the reduced graphene oxide-CS (rGO-CS) nanocomposites with capacity to resist high load, but the weak HB within the organic matrix of CS hindered the stress

Y. Cheng, Dr. J. Peng, H. Xu, Prof. Q. Cheng
Key Laboratory of Bio-inspired Smart Interfacial Science and Technology of Ministry of Education
School of Chemistry
Beijing Advanced Innovation Center for Biomedical Engineering
Beihang University
Beijing 100191, P. R. China
E-mail: cheng@buaa.edu.cn
Prof. Q. Cheng
State Key Laboratory for Modification of Chemical Fibers and Polymer Materials
Donghua University
Shanghai 201620, P. R. China
Prof. Q. Cheng
State Key Laboratory of Organic-Inorganic Composites
Beijing University of Chemical Technology
Beijing 1000029, P. R. China
The ORCID identification number(s) for the author(s) of this article can be found under https://doi.org/10.1002/adfm.201800924.

DOI: 10.1002/adfm.201800924

© 2018 WILEY-VCH Verlag GmbH & Co. KGaA, Weinheim

transferring between the CS chains, resulting in an obstacle to further improve the tensile strength. Previous works have demonstrated that the IB is effective for designing synergistic interfacial interaction to improve mechanical properties of BGBNs.[3,4] However, as the short bond length and weak bond energy of IB, conventionally at an interlayered motif, restrict the load transferring between GO nanosheets when under tensile stress.[4] Herein, inspired by *Glycera*, the special synergistic interfacial interactions have been demonstrated. As the strong binding affinity of Cu for the CS chains is much higher,[15] thus we select copper ions to achieve synergistic effect. The copper ions are introduced into the CS matrix to form the metal–ligand coordinate bonds, which specifically cross-link the CS chains and improve the stress transferring. The resultant tensile strength of this *Glycera*-inspired nanocomposites reaches up to record 868.6 MPa, which is five times higher than that of the pure rGO film. The superiority of *Glycera*-inspired strategy is also demonstrated by the comparative samples with interlayered IB between GO nanosheets. Meanwhile, the resultant BGBN integrates the relatively high electrical conductivity with 234.8 ± 14.4 S cm^{-1}. The *Glycera*-inspired strategy of synergistic interfacial interactions promises a creative method to fabricate high-performance BGBNs.

2. Results and Discussion

The fabrication process of BGBNs is illustrated in **Figure 1**a. First, the copper chloride solution was added to CS solution to obtain CS/Cu chelated hybrid.[15] Then, the exfoliated GO monolayer nanosheets with a thickness of ≈1.0 nm (Figure S1, Supporting Information) and lateral size of ≈3.5 µm (Figure S2, Supporting Information) was mixed with the CS/Cu solution to obtain the GO/CS/Cu building blocks. After vacuum-assisted filtration, the building blocks were assembled into the GO-CS-Cu layered nanocomposites. During this process, the CB between CS and GO nanosheets is formed via the amidation and ring-opening reaction.[14] And the CS/Cu chelated structure is also retained. Finally, the GO-CS-Cu nanocomposites were chemically reduced through hydroiodic acid (HI)[16] to remove the redundant oxygen-containing functional groups on GO nanosheets, leading to the conductive rGO-CS-Cu nanocomposites, as shown in Figure 1b. The cross-sectional scanning electron microscopy (SEM) image of rGO-CS-Cu nanocomposites in Figure 1c indicates a nacre-like lamellar structure. Four kinds of GO-CS nanocomposites were fabricated with different CS contents to optimize mechanical properties of GO-CS nanocomposites, named as GO-CS-1

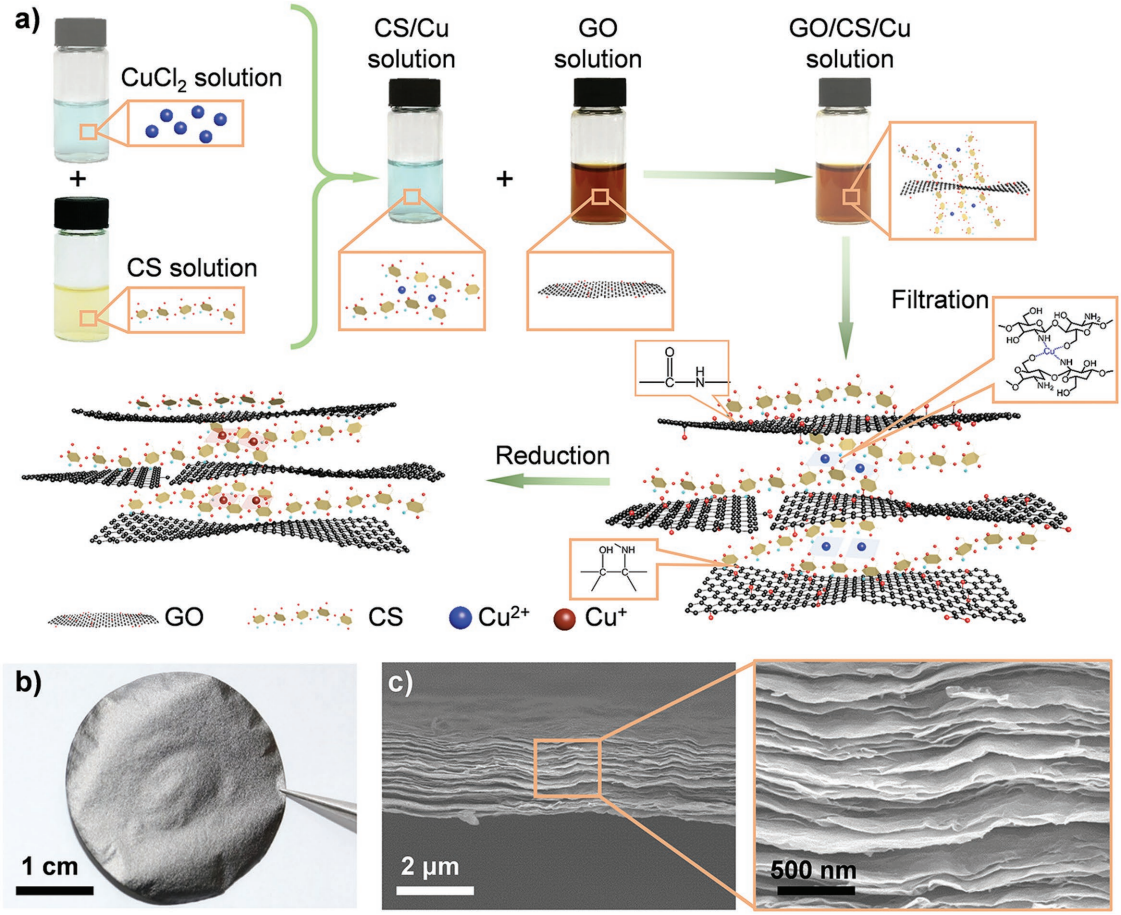

Figure 1. a) The illustration of fabrication method for rGO-CS-Cu nanocomposites. The $CuCl_2$ solution was first mixed with CS. Then CS/Cu hybrid solution was added into GO solution to obtain GO/CS/Cu building blocks. Subsequently, the building blocks were assembled into GO-CS-Cu nanocomposites and finally chemically reduced by HI to obtain rGO-CS-Cu nanocomposites. b) The digital photograph and c) SEM photograph of cross-section morphology of rGO-CS-Cu nanocomposites.

© 2018 WILEY-VCH Verlag GmbH & Co. KGaA, Weinheim

(GO:CS = 97.4:2.6), GO-CS-2 (GO:CS = 95.1:4.9), GO-CS-3 (GO:CS = 93.5:6.5), and GO-CS-4 (GO:CS = 91.2:8.8), respectively. The results indicate that the maximum tensile strength of 543.0 ± 60.7 MPa can be obtained in GO-CS nanocomposites with 6.5 wt% CS. Then, the GO-CS represents GO-CS-3 nanocomposites in the following. The GO-CS-Cu nanocomposites with a series contents of cooper ions were fabricated based on the optimized GO-CS nanocomposites, designated as GO-CS-Cu-I (GO:Cu = 99.0:1.0), GO-CS-Cu-II (GO:Cu = 98.0:2.0), GO-CS-Cu-III (GO:Cu = 97.5:2.5), and GO-CS-Cu-IV (GO:Cu = 97.0:3.0), respectively. And GO-Cu nanocomposites were also fabricated with the copper ions of 2.5 wt% for comparison. The thermogravimetric analysis (TGA) was used to calculate the exact content of copper ions, as shown in Figure S3 and Tables S1 and S2 (Supporting Information).

The X-ray diffraction (XRD) spectra are demonstrated in Figure S4 (Supporting Information), and the exact *d*-spacing values are listed in Tables S3 and S4 (Supporting Information). The *d*-spacing of GO-CS nanocomposites is 8.76 Å, much higher than that of GO film (7.66 Å), indicating the successful insert of CS into GO interlayers.[14] While the *d*-spacing of GO-CS-Cu-III nanocomposites decreases surprisingly to 8.56 Å, compared with 8.76 Å of GO-CS nanocomposites, revealing that the inserted CS chains have been highly packed by copper ions. After HI reduction, the *d*-spacing of resultant nanocomposites decreases due to the removal of the residual oxygen containing functional groups on the surface of GO nanosheets,[17] which can also be proved via Raman spectra as the I_D/I_G ratio increases apparently after reduction (see Figure S5 and Table S5, Supporting Information).[18] Correspondingly, the I_D/I_G ratio of GO-CS-Cu-III nanocomposites is 1.05, lower than that of GO-CS nanocomposites with the value of 1.18, which also indicates a more orderly layered structure of GO-CS-Cu-III nanocomposites was achieved.[18]

To verify the interactions between GO and CS, several characterizations have been done. The Fourier transform infrared (FTIR) measurements are performed to identify the chemical reactions between CS and GO, as shown in **Figure 2**a. The characteristic peaks of stretch vibration at 1261 cm^{-1} for C—N are attributed to not fully deacetylated amide groups of CS.[14] This peak shifts to 1230 cm^{-1} in GO-CS and GO-CS-Cu-III nanocomposites, elucidating the transition from amine groups to amide groups.[14] Furthermore, epoxide ring-opening in GO-CS-Cu-III is demonstrated in FTIR spectrum as the disappearance of epoxy C—O groups (1222 cm^{-1}) in Figure 2a.[3b] The broad C1s peak of GO-CS-Cu-III could be divided into five peaks at 288.9, 287.7, 286.6, 286.1, 285.5, and 284.4 eV, corresponding to C(O)O, C=O, C(O)C, C–N, C—OH and C—C, respectively, as shown in Figure 2b. The decrease of C—O peak intensity in GO-CS-Cu-III nanocomposites compared with GO (Figure S6, Supporting Information) further confirms the ring-opening reaction on surface of GO nanosheets.[19] After reduction,

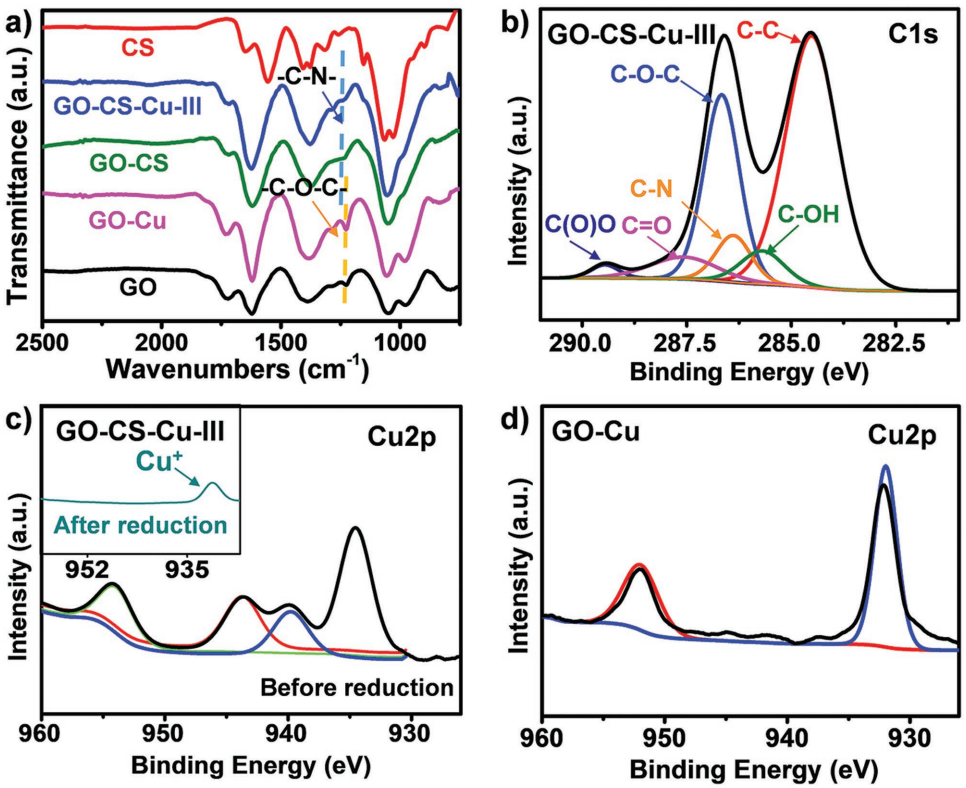

Figure 2. a) FTIR spectra of GO, CS, GO-CS, GO-Cu, and GO-CS-Cu-III nanocomposites. The peaks at 1230 cm^{-1} in GO-CS-Cu-III indicate the formation of amide groups. Epoxide ring-opening in GO-CS-Cu-III is demonstrated as the disappearance of epoxy C—O groups (1222 cm^{-1}). b) XPS spectrum of GO-CS-Cu-III nanocomposites. The decrease of C—O—C peak intensity at 286.7 eV corroborates the ring-opening in GO-CS-Cu-III. c) XPS spectrum of Cu2p in GO-CS-Cu-III nanocomposites before and after reduction. Before reduction, two main peaks with shakeup satellite peaks confirm the chelation of Cu(II) on CS. And the peak after reduction indicates the transform of Cu(II) to Cu(I). d) XPS spectrum of Cu2p in GO-Cu nanosheets.

© 2018 WILEY-VCH Verlag GmbH & Co. KGaA, Weinheim

redundant oxygen-containing functional groups are removed as shown in Figure S6 (Supporting Information), as the intensity of C(O)O, C=O, C(O)C, C−OH decreases. While in N1s X-ray photoelectron spectroscopy (XPS) spectra of GO-CS, rGO-CS, GO-CS-Cu-III, and rGO-CS-Cu-III nanocomposites, the peaks at around 400.2 eV retain in these nanocomposites (Figure S7, Supporting Information), indicating the retention of amide groups, which is formed as the reaction between GO and CS. The increased intensity of peaks for protonated amine in nanocomposites after reduction is caused by the acid circumstance.

In Cu2p XPS spectra of GO-CS-Cu-III nanocomposites, the copper ions mainly exist on bivalent stage before reduction. A large symmetric binding energy (BE) peak with a maximum at 934.6 eV is assigned to core feature,[20] accompanied by the characteristic Cu(II) shakeup satellite peaks at 939.9 and 943.7 eV, as shown in Figure 2c.[21] The existence of satellite peaks demonstrates the formation of chelation in tetrahedral sites between CS and Cu.[22] The core peaks of GO-Cu nanocomposites exist at 952.0 and 932.2 eV, as shown in Figure 2d, which is totally different from the peaks of GO-CS-Cu-III at 954.3 and 934.6 eV, indicating that the copper ions in GO-CS-Cu-III chelate with CS, rather than GO nanosheets as in GO-Cu nanocomposites. After reduction, the Cu(II) was reduced to Cu(I) by HI as the BE peak of Cu(I) appears at 931.0 eV, which shifts to a lower BE peak compared with the theoretical value of 932.0 eV, due to chelation with amino groups and hydroxyl groups in CS.[22]

The mechanical and electrical properties of *Glycera*-inspired rGO-CS-Cu nanocomposites are also impressive. The stress–strain curves of the resultant nanocomposites are presented in **Figure 3**a and the detailed data are listed in Table S6 (Supporting Information). The mechanical properties of rGO-CS-Cu nanocomposites with different contents of copper ions are exhibited in Figure 3b. The copper ion content of optimized GO-CS-Cu-III nanocomposites is ≈2.5 wt%, which is consistent with the content of copper ions in the jaw of *Glycera*. The tensile strength and toughness of rGO-CS-Cu-III nanocomposites reach up to record 868.6 ± 40.6 MPa and 14.0 ± 1.2 MJ m^{-3}, respectively. The extremely high tensile strength of rGO-CS-Cu-III nanocomposites attains almost five times higher than that of pure rGO film (173.6 ± 7.4 MPa). The fracture morphology of rGO-CS-Cu-III nanocomposites shows the clear pull-out of rGO nanosheets and abundant curved edges as shown in Figure 3c, demonstrating that the main fracture mode of rGO-CS-Cu-III nanocomposites is the

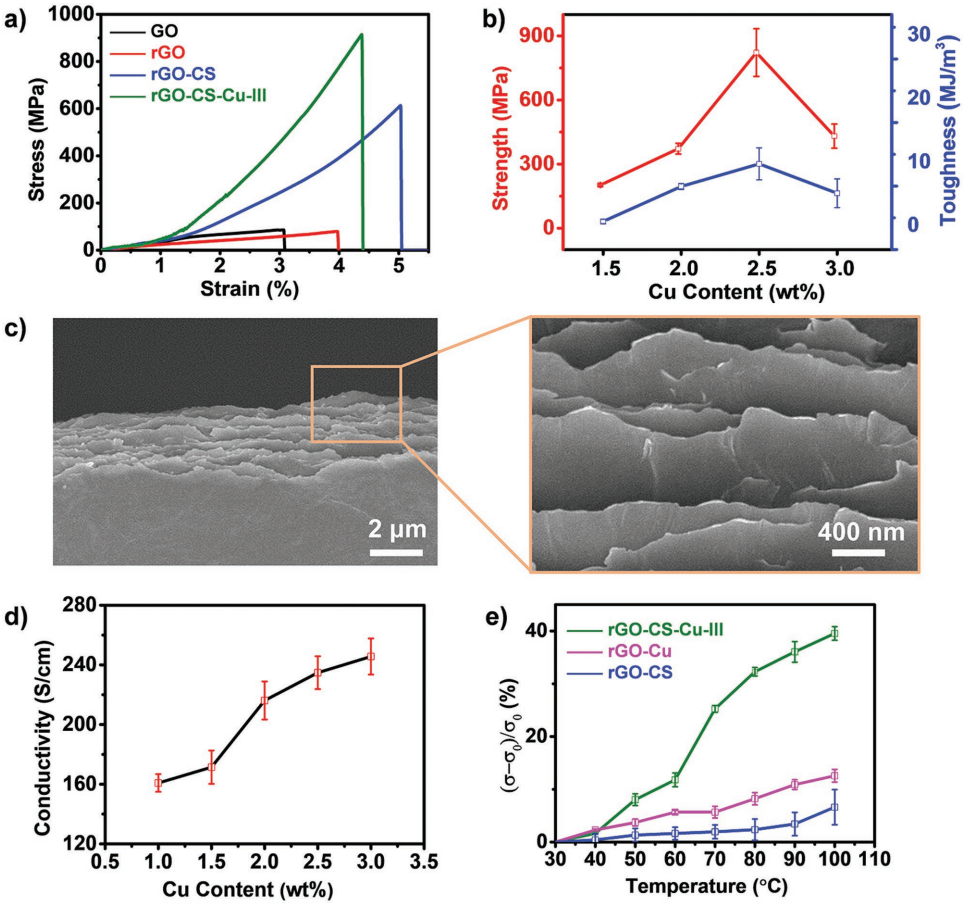

Figure 3. Mechanical and electrical properties. a) Stress–strain curves of GO film, rGO film, rGO-CS, and rGO-CS-Cu-III. b) The tensile strength and toughness of rGO-CS-Cu nanocomposites with different Cu contents. c) The fracture morphology of rGO-CS-Cu-III. d) Electrical conductivities of rGO-CS-Cu nanocomposites with different contents of copper ions. e) Patterns of electrical conductivities with the elevation of temperature of rGO-CS-Cu-III, rGO-Cu, and rGO-CS. σ refers to the electrical conductivities of nanocomposites at temporal temperature, and σ_0 refers to the electrical conductivities of nanocomposites at 30 °C.

© 2018 WILEY-VCH Verlag GmbH & Co. KGaA, Weinheim

shear rupture of interfaces induced by the slippage of rGO nanosheets in accordance with previous work.[1c] Fracture morphologies of different rGO-CS or rGO-CS-Cu nanocomposites are displayed in Figures S8 and S9 (Supporting Information). Except for mechanical properties, the rGO-CS-Cu nanocomposites also possess relatively high electrical conductivities which increase with the rise of copper ion contents as shown in Figure 3d. The corresponding data are listed in Table S7 (Supporting Information). The electrical conductivity of rGO-CS-Cu-III nanocomposites reaches 234.8 S cm^{-1}, which is nearly as high as rGO film (254.9 S cm^{-1}). The electrical conductivity benefits from the migration of copper ions among the CS matrix, which could be proved by the correlation between conductivity and temperature. As shown in Figure 3e, the electrical conductivity of rGO-CS-Cu nanocomposites increases more sharply than those of rGO-CS and rGO-Cu nanocomposites with the rise of temperature. This is because that the thermally enhanced complezation-decomplezation process of CS/Cu chelated hybrid and segmental motion of CS leads to the higher migration rate of copper ions.[5,23]

The high mechanical properties of rGO-CS-Cu nanocomposites are attributed to *Glycera*-inspired synergistic multiple interactions. To further explore the mechanism of the synergistic interactions, rGO-CS-Cu nanocomposites were fabricated through other two different methods as the control samples, designated as rGO-CS-Cu-A and rGO-CS-Cu-B, which is illustrated in Figure S10 (Supporting Information). To fabricate GO-CS-Cu-A nanocomposites, the copper chloride was added into GO solution, followed by the addition of CS solution. During this process, the copper ions are first chelated with GO nanosheets and fail to interact with the following CS as shown in **Figure 4**a, proved by the accordance of XPS spectra with GO-Cu (Figure 2d). What's more, the oxygen-containing groups on GO occupied by copper ions are also unable to covalently react with CS chains demonstrated by the FTIR spectrum with the absence of peak at 1230 cm^{-1} as shown in Figure 4b.[14] While the GO-CS-Cu-B nanocomposites were built through assembling the GO/CS homogenous suspension with copper chloride solution, where the CS first covalently cross-link the GO nanosheets and cannot chelate the subsequent copper ions with the evidence of FTIR characteristic peak at 1230 cm^{-1} (Figure 4b) and XPS spectra of GO-CS-Cu-B nanocomposites (Figure 4a), the same with GO-Cu nanocomposites (Figure 2d). As shown in Figure 4c, the rGO-CS-Cu-A and rGO-CS-Cu-B nanocomposites exhibit the tensile strength of 434.8 ± 18.2 and 437.4 ± 9.3 MPa, respectively, while the rGO-CS-Cu-III nanocomposites possess the most admirable tensile strength as high as 868.6 ± 40.6 MPa.

The discrepancy among the tensile strengths of these three kinds of rGO-CS-Cu nanocomposites is caused by the different interfacial interactions between rGO nanosheets. Conclusively, rGO-CS-Cu-A nanocomposites combine HB with IB as copper ions chelated with GO nanosheets. The rGO-CS-Cu-B nanocomposites are fabricated with CB between GO and CS, as well

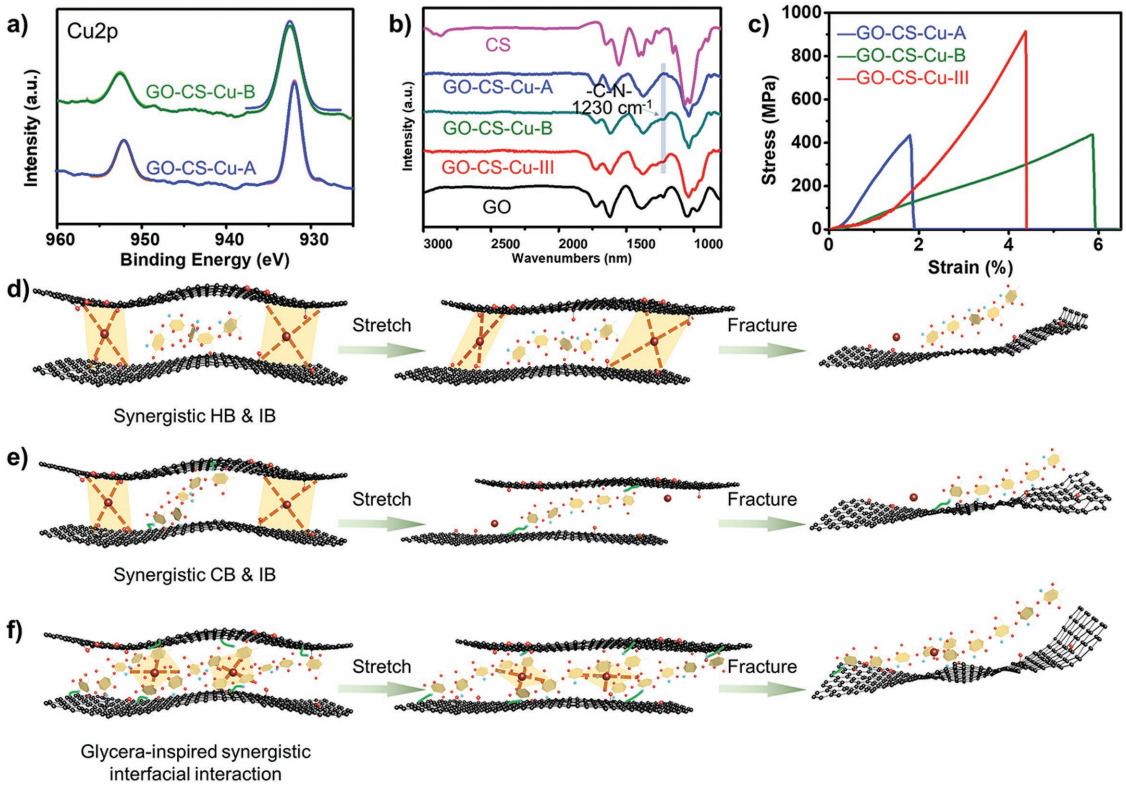

Figure 4. Fracture mechanisms of three rGO-CS-Cu nanocomposites with different fabricating methods. a) XPS spectra of Cu2p of GO-CS-Cu-A and GO-CS-Cu-B. b) FTIR spectra of GO-CS-Cu-A, GO-CS-Cu-B, GO-CS-Cu-III, GO, and CS. The peaks at 1230 cm^{-1} in GO-CS-Cu-III and GO-CS-Cu-B indicate the formation of amide group. c) Stress–strain curves of GO-CS-Cu nanocomposites fabricated with different methods. d–f) Three different fracture mechanisms of rGO-CS-Cu-A, rGO-CS-Cu-B, and rGO-CS-Cu-III, respectively.

© 2018 WILEY-VCH Verlag GmbH & Co. KGaA, Weinheim

as interlayer IB. And the rGO-CS-Cu-III nanocomposites mimic the unique chelation structure of *Glycera* to form the special interface combination of IB and CB, as the copper ions chelated with CS, and CS cross-linking onto GO nanosheets. As demonstrated in Figure 4d, mutual slippage of rGO nanosheets in rGO-CS-Cu-A nanocomposites is initiated by the loading stress. The relatively weak HB is first damaged, followed by intercalated IB. Thus, the interfacial interactions are destroyed, before being able to transfer stress to rGO nanosheets, engendering a brittle fracture. In rGO-CS-Cu-B nanocomposites, the mutual slippage of rGO nanosheets induces the stretch of CS chains anchored onto the nanosheets, and intercalated IB is broken to dissipate much of loading energy as shown in Figure 4e. But the damaged IB may cause the surrounding CS matrix to suffer the stress concentration due to the independent formation of IB and CB, which confines the improvement of tensile strength. Rather than the intercalated IB as former two nanocomposites, the IB in rGO-CS-Cu-III nanocomposites is chelated with CS chains, forming *Glycera*-inspired interface design with a uniform and continuous CS/Cu hybrid matrix. As shown in Figure 4f, with the shear of rGO nanosheets, the copper ions between CS chains retard the stretch of CS chains. During this process, the effective stiffening of CS matrix is formed due to the constrained motion of polymer chains.[24] The stress can be transferred throughout the CS/Cu matrix via IB and furthermore channeled into rGO nanosheets with the assistance of CB, which forms a stronger interfacial interaction for bearing the load. With the intensified slippage of rGO nanosheets, the IB begins to be damaged, while the uniformly continuous Cu/CS matrix also avoids the defects caused by damaged IB. Eventually, destruction of CB induces the total fracture. The *Glycera*-inspired synergistic design confers the rGO-CS-Cu-III nanocomposites with efficient stress transferring, leading to extremely high tensile strength.

The *Glycera*-inspired interface design brings out a huge advantage than conventional synergistic effect in previous graphene-based nanocomposites. As demonstrated in **Figure 5**, the rGO-CS-Cu-III nanocomposites possess higher tensile strength than natural nacre and other graphene-based nanocomposites including BGBNs with HB, such as GO-poly(vinyl alcohol) (GO-PVA),[25] rGO-PVA,[26] GO-poly(methyl methacrylate) (GO-PMMA),[25] and rGO- polyacrylic acid (rGO-PAA);[27] with IB, such as rGO-Cu,[28] GO-Ca,[4] GO-Mg,[4] rGO-Al,[29] and rGO-Zn;[30] with CB, such as GO-glutaraldehyde (GO-GA),[31] GO-borate,[32] polydopamine-capped GO-polyetherimide (PGO-PEI),[33] rGO-10,12-pentacosadiyn-1-ol (rGO-PCDO);[34] as well as via synergistic effect, such as rGO-poly(acrylic acid-*co*-(4-acrylamidophenyl)boronic acid) (rGO-PAPB),[35] rGO-polydopamine (rGO-PDA),[36] GO-silk fibroin (GO-SL),[37] rGO-SL,[38] and rGO with almost intact basal plane-cellulose nanocrystal (ai-rGO-CNC),[2] GO-cellulose nanocrystal (GO-CNC),[39] rGO-CNC,[39] rGO-CS,[14] rGO-double-wall carbon nanotubes-PCDO (rGO-DWNT-PCDO),[40] rGO-molybdenum disulfide-thermoplastic polyurethanes (rGO-MoS_2-TPU),[41] rGO-montmorillonite-PVA (rGO-MMT-PVA),[42] GO-polyetherimide (GO-PEI),[43] rGO-DWNT-PVA,[44] rGO-PCDO-Zn,[3b] rGO-hydroxypropyl cellulose-Cu (rGO-HPC-Cu),[3a] and rGO-PDA-Ni.[3c] The certain mechanical properties are listed in

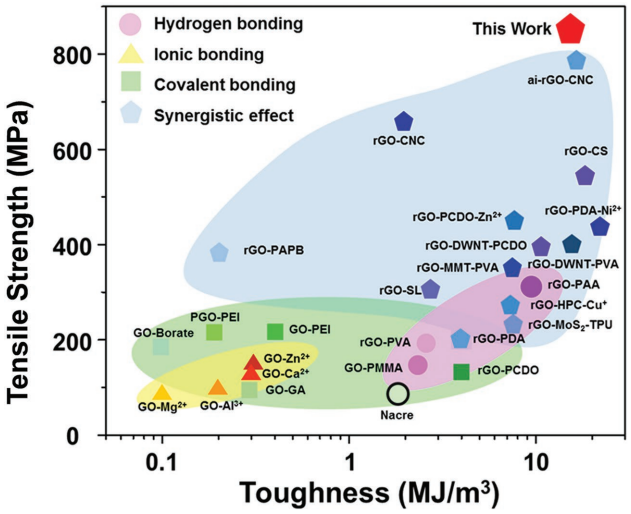

Figure 5. Comparison of tensile strength and toughness of rGO-CS-Cu-III nanocomposites with other layered materials. The typical BGBNs with HB are presented as pink circles, and IB as yellow triangle, CB as green squares, and synergistic effect as blue pentagon. The rGO-CS-Cu-III possesses the best tensile strength among these BGBNs.

Table S8 (Supporting Information). Generally, the BGBNs with synergistic effect function higher performance than other BGBNs with the single interfacial interaction.[45] Compared with other IB-containing synergistic interfacial interactions, this work possesses much higher tensile strength through fabricating synergistic interface inspired by the jaw of *Glycera*. The mechanism of rGO-HPC-Cu[3a] is similar to that of rGO-CS-Cu-A while the rGO-PCDO-Zn[3b] and rGO-PDA-Ni[3c] also resemble the rGO-CS-Cu-B nanocomposites. Both achieve considerable improvement on tensile strength through some strong IB. However, IB and other interactions may perform in a relatively independent way leading to less efficient stress transferring, which hinders the further promotion on tensile strength. Except for synergistic interfacial interactions, the nanocomposites based on synergistic building blocks also reach high mechanical properties. For example, the ai-rGO-CNC[2] reaches the tensile strength as high as 765 MPa, which benefits from the large lateral size (≈14 µm).[46] The wrinkled structures caused by CNC nanofibers perform as an interlocked interface, which impedes the mutual slippage of GO nanosheets and thus also promotes the tensile strength. The formation of wrinkled structures, however, is difficult to be controlled, which may cause inevitable defects of layered structure. *Glycera*-inspired synergistic interfacial interactions demonstrate the capability to effectively transfer the load stress and simultaneously minimize the defects. What's more, our fabrication strategy is also simple and suitable for large-scale applications.

3. Conclusion

Glycera-inspired synergistic interfacial interactions have been utilized to construct the ultrastrong nanocomposites with a record tensile strength of 868.6 ± 40.6 MPa. Different from the former works that the ions mainly chelated with GO nanosheets

© 2018 WILEY-VCH Verlag GmbH & Co. KGaA, Weinheim

directly, the special *Glycera*-inspired interface design is achieved with the help of the IB from the metal–ligand bonds between copper ions and CS matrix as well as the CB between the CS chains and rGO nanosheets. Creative finding in this work is that the highly effective transferring of *Glycera*-inspired interface contributes to the significant promotion of tensile strength, which is distinguished from traditional IB. Comparative samples with interlayered IB were also used to demonstrate the superiority of *Glycera*-inspired strengthening mechanism. Furthermore, the introduction of copper ion also benefits for the electrical conductivity reaching up to 234.8 ± 14.4 S cm^{-1}. This nacre-like BGBN with *Glycera*-inspired interface with impressive mechanical and electrical properties is promising for applications in many fields such as flexible energy devices, supercapacitors, and other electronic devices.

4. Experimental Section

Materials: Graphene oxide was prepared by a modified Hummer's method. Chitosan (medium molecular weight, 75–85% deacetylated), 57 wt% HI, and copper chloride (analytically pure) were purchased from Sigma-Aldrich. Sodium hydroxide (analytically pure), potassium permanganate (analytically pure), sodium nitrate (analytically pure), sulfuric acid (analytically pure), graphite powder (analytically pure), and ethyl alcohol (analytically pure) were purchased from Beijing Chemical Factory. All the reagents were used without further purification.

Preparation of GO Solution: The graphite powder was mixed with sodium nitrate and sulfuric acid, then stirred for 1 h. 6 g potassium permanganate was added rather slowly at a speed of 1 g min^{-1}. After stirring for 4 h, 300 mL deionized water was added drop by drop into the mixture, followed by stirring at 35 °C for 30 min. The mixture was then poured into 60 °C deionized water, and finally 35% hydrogen peroxide was added to confirm the successful oxidation. The mixture was laid aside for 2 d and washed through centrifugation with 30% hydrochloric acid for three times and with water for three times. The GO solution was finally obtained.

Fabrication of CS/Cu Hybrid Solution: The CS was dispersed in 2% acetic acid solution with a concentration of 10 mg mL^{-1} and stirred for two weeks. Copper chloride was dispersed in deionized water with a concentration of 0.5 mg mL^{-1}, followed by the copper chloride solution being added to the CS solution drop by drop with continuous stirring. The mixture was stirred for 30 h at room temperature for further interaction.

Fabrication of GO/CS/Cu Building Blocks: The GO was dispersed in deionized water with a concentration of 1.5 mg mL^{-1} and stirred for 24 h to form a homogenous suspension. Then the CS/Cu solution was dropped slowly with certain ratios into the GO solution followed by sonication for 15 min. 79 µL, 0.5 mg mL^{-1} sodium hydroxide solution was added to neutralize the acetic acid solution, followed with another 5 µL to stabilize these suspensions. And the pH value of these suspensions is controlled around 10.

Fabrication of rGO-CS-Cu Nanocomposites: Homogeneous suspension of GO/CS/Cu building blocks was assembled into GO-CS-Cu nanocomposites via vacuum filtration. And GO-CS-Cu nanocomposites were chemically reduced by hydroiodic acid for 18 h, then washing with ethanol for nearly 3 d.

Characterization: Mechanical properties were measured on a Shimadzu AGS-X Tester with a loading rate of 1 mm min^{-1} under a 20 N load cell. All measurements were conducted at room temperature. The samples were cut into strips with a length of 8 mm and a width of 3 mm. The thickness of all samples was confirmed by SEM. SEM images were recorded by a Hitachi S-4800 at 11.5 kV after sputtering a thin Pt/Au coating onto the samples. The values of tensile strength and strain were accounted by the stress–strain curves, and the values of toughness were calculated by the integral area under the curves. The mechanical properties for each sample were based on the average values of 3–5 specimens.

Atomic force microscopy (AFM) was conducted by a Leica TCS SP5. The GO solution was diluted into 0.05 mg mL^{-1} with pure deionized water. Then, the solution was dropped on freshly cleaved mica and dried at room temperature for nearly 24 h to obtain the samples for the AFM measurement. TGA was performed on TG/DTA6300, NSK with a temperature elevation rate of 10 K min^{-1} under nitrogen. This measurement was taken from 25 to 800 °C. Raman spectroscopy measurements were recorded using a LabRAM HR800 (Horiba JobinYvon). FTIR measurements were conducted by a Thermo Nicolet Nexus-470 FTIR instrument in the attenuated total reflection (ATR) mode. XPS tests were carried out in an ESCALab220i-XL (ThermoScientific) with a monochromatic Cu Kα X-ray source. XRD measurements were taken with Cu Kα radiation; λ = 0.154 nm (1.54 Å). The measurements were conducted under a voltage of 40.0 kV, a current of 30.0 mA, and a scanning speed of 5.0° min^{-1}. The electrical conductivities were tested by a standard two-probe method using a source meter (Agilent E4980A). The samples were prepared as strips with the width of 3 mm and the length of around 5 cm.

Supporting Information

Supporting Information is available from the Wiley Online Library or from the author.

Acknowledgements

Y.C., J.P., and H.X. contributed equally to this work. This work was supported by the Excellent Young Scientist Foundation of NSFC (51522301), the National Natural Science Foundation of China (21273017, 51103004), the Program for New Century Excellent Talents in University (NCET-12-0034), the Fok Ying-Tong Education Foundation (141045), the 111 Project (B14009), the Aeronautical Science Foundation of China (20145251035, 2015ZF21009), State Key Laboratory of Organic-Inorganic Composites, Beijing University of Chemical Technology (oic-201701007), the State Key Laboratory for Modification of Chemical Fibers and Polymer Materials, Donghua University (LK1710), the Fundamental Research Funds for the Central Universities (YWF-16-BJ-J-09, YWF-17-BJ-J-33), and the Academic Excellence Foundation of BUAA (20170666) for Ph.D. students.

Conflict of Interest

The authors declare no conflict of interest.

Keywords

bioinspired materials, *Glycera*, graphene oxide, nacre, synergistic interfacial interactions

Received: February 4, 2018
Revised: February 24, 2018
Published online: April 10, 2018

[1] a) S. Gong, H. Ni, L. Jiang, Q. Cheng, *Mater. Today* **2017**, *20*, 210; b) Y. Zhang, S. Gong, Q. Zhang, P. Ming, S. Wan, J. Peng, L. Jiang, Q. Cheng, *Chem. Soc. Rev.* **2016**, *45*, 2378; c) J. Wang, Q. Cheng, Z. Tang, *Chem. Soc. Rev.* **2012**, *41*, 1111; d) S. Wan, J. Peng, L. Jiang, Q. Cheng, *Adv. Mater.* **2016**, *28*, 7862; e) Q. Cheng, J. Duan, Q. Zhang, L. Jiang, *ACS Nano* **2015**, *9*, 2231; f) Q. Cheng, L. Jiang, Z. Tang, *Acc. Chem. Res.* **2014**, *47*, 1256.
[2] Y. Wen, M. Wu, M. Zhang, C. Li, G. Shi, *Adv. Mater.* **2017**, *29*, 1702831.

© 2018 WILEY-VCH Verlag GmbH & Co. KGaA, Weinheim

[3] a) Q. Zhang, S. Wan, L. Jiang, Q. Cheng, *Sci. China: Technol. Sci.* **2016**, *60*, 758; b) S. Gong, L. Jiang, Q. Cheng, *J. Mater. Chem. A* **2016**, *4*, 17073; c) S. Wan, F. Xu, L. Jiang, Q. Cheng, *Adv. Funct. Mater.* **2017**, *27*, 1605636.
[4] S. Park, K. Lee, G. Bozoklu, W. Cai, S. T. Nguyen, R. S. Ruoff, *ACS Nano* **2008**, *2*, 572.
[5] C. Zhang, S. Gamble, D. Ainsworth, A. M. Slawin, Y. G. Andreev, P. G. Bruce, *Nat. Mater.* **2009**, *8*, 580.
[6] M. J. Harrington, H. S. Gupta, P. Fratzl, J. H. Waite, *J. Struct. Biol.* **2009**, *167*, 47.
[7] D. S. Hwang, H. Zeng, A. Masic, M. J. Harrington, J. N. Israelachvili, J. H. Waite, *J. Biol. Chem.* **2010**, *285*, 25850.
[8] S. Weiner, L. Addadi, *Science* **2002**, *298*, 375.
[9] H. C. Lichtenegger, T. Schöberl, M. H. Bartl, H. Waite, G. D. Stucky, *Science* **2002**, *298*, 389.
[10] P. Gibbs, G. Bryan, *J. Mar. Biol. Assoc. UK* **1980**, *60*, 205.
[11] D. N. Moses, J. H. Harreld, G. D. Stucky, J. H. Waite, *J. Biol. Chem.* **2006**, *281*, 34826.
[12] a) D. N. Moses, M. G. Pontin, J. H. Waite, F. W. Zok, *Biophys. J.* **2008**, *94*, 3266; b) M. G. Pontin, D. N. Moses, J. H. Waite, F. W. Zok, *Proc. Natl. Acad. Sci. USA* **2007**, *104*, 13559.
[13] M. Rinaudo, *Prog. Polym. Sci.* **2006**, *31*, 603.
[14] S. Wan, J. Peng, Y. Li, H. Hu, L. Jiang, Q. Cheng, *ACS Nano* **2015**, *9*, 9830.
[15] Z. Sun, F. Lv, L. Cao, L. Liu, Y. Zhang, Z. Lu, *Angew. Chem., Int. Ed.* **2015**, *54*, 7944.
[16] S. Pei, J. Zhao, J. Du, W. Ren, H. Cheng, *Carbon* **2010**, *48*, 4466.
[17] D. R. Dreyer, S. Park, C. W. Bielawski, R. S. Ruoff, *Chem. Soc. Rev.* **2010**, *39*, 228.
[18] K. N. Kudin, B. Ozbas, H. C. Schniepp, R. K. Prud'Homme, I. A. Aksay, R. Car, *Nano Lett.* **2008**, *8*, 36.
[19] O. C. Compton, D. A. Dikin, K. W. Putz, L. C. Brinson, S. T. Nguyen, *Adv. Mater.* **2010**, *22*, 892.
[20] a) L. Dambies, C. Guimon, S. Yiacoumi, E. Guibal, *Colloids Surf., A* **2001**, *177*, 203; b) K. L. Deutsch, B. H. Shanks, *J. Catal.* **2012**, *285*, 235.
[21] R. S. Vieira, M. L. M. Oliveira, E. Guibal, E. Rodríguez-Castellón, M. M. Beppu, *Colloids Surf., A* **2011**, *374*, 108.
[22] P. Liu, E. J. M. Hensen, *J. Am. Chem. Soc.* **2013**, *135*, 14032.
[23] G. S. MacGlashan, Y. G. Andreev, P. G. Bruce, *Nature* **1999**, *398*, 792.
[24] P. Podsiadlo, A. K. Kaushik, E. M. Arruda, A. M. Waas, B. S. Shim, J. Xu, H. Nandivada, B. G. Pumplin, J. Lahann, A. Ramamoorthy, *Science* **2007**, *318*, 80.
[25] K. W. Putz, O. C. Compton, M. J. Palmeri, S. T. Nguyen, L. C. Brinson, *Adv. Funct. Mater.* **2010**, *20*, 3322.
[26] Y. Li, T. Yu, T. Yang, L. Zheng, K. Liao, *Adv. Mater.* **2012**, *24*, 3426.
[27] S. Wan, H. Hu, J. Peng, Y. Li, Y. Fan, L. Jiang, Q. Cheng, *Nanoscale* **2016**, *8*, 5649.
[28] J. Hwang, T. Yoon, S. H. Jin, J. Lee, T.-S. Kim, S. H. Hong, S. Jeon, *Adv. Mater.* **2013**, *25*, 6724.
[29] C. Yeh, K. Raidongia, J. Shao, Q. Yang, J. Huang, *Nat. Chem.* **2015**, *7*, 166.
[30] D. V. Lam, T. Gong, S. Won, J. Kim, H. Lee, C. Lee, S. Lee, *Chem. Commun.* **2015**, *51*, 2671.
[31] Y. Gao, L. Liu, S. Zu, K. Peng, D. Zhou, B. Han, Z. Zhang, *ACS Nano* **2011**, *5*, 2134.
[32] Z. An, O. C. Compton, K. W. Putz, L. C. Brinson, S. T. Nguyen, *Adv. Mater.* **2011**, *23*, 3842.
[33] Y. Tian, Y. Cao, Y. Wang, W. Yang, J. Feng, *Adv. Mater.* **2013**, *25*, 2980.
[34] Q. Cheng, M. Wu, M. Li, L. Jiang, Z. Tang, *Angew. Chem., Int. Ed.* **2013**, *52*, 3750.
[35] M. Zhang, L. Huang, J. Chen, C. Li, G. Shi, *Adv. Mater.* **2014**, *26*, 7588.
[36] W. Cui, M. Li, J. Liu, B. Wang, C. Zhang, L. Jiang, Q. Cheng, *ACS Nano* **2014**, *8*, 9511.
[37] K. Hu, M. K. Gupta, D. D. Kulkarni, V. V. Tsukruk, *Adv. Mater.* **2013**, *25*, 2301.
[38] K. Hu, L. S. Tolentino, D. D. Kulkarni, C. Ye, S. Kumar, V. V. Tsukruk, *Angew. Chem., Int. Ed.* **2013**, *52*, 13784.
[39] R. Xiong, K. Hu, A. M. Grant, R. Ma, W. Xu, C. Lu, X. Zhang, V. V. Tsukruk, *Adv. Mater.* **2016**, *28*, 1501.
[40] S. Gong, W. Cui, Q. Zhang, A. Cao, L. Jiang, Q. Cheng, *ACS Nano* **2015**, *9*, 11568.
[41] S. Wan, Y. Li, J. Peng, H. Hu, Q. Cheng, L. Jiang, *ACS Nano* **2015**, *9*, 708.
[42] P. Ming, Z. Song, S. Gong, Y. Zhang, J. Duan, Q. Zhang, L. Jiang, Q. Cheng, *J. Mater. Chem. A* **2015**, *3*, 21194.
[43] Z. Tan, M. Zhang, C. Li, S. Yu, G. Shi, *ACS Appl. Mater. Interfaces* **2015**, *7*, 15010.
[44] S. Gong, M. Wu, L. Jiang, Q. Cheng, *Mater. Res. Express* **2016**, *3*, 075002.
[45] Q. Cheng, L. Jiang, *Sci. China Mater.* **2016**, *59*, 889.
[46] P. Das, J. M. Malho, K. Rahimi, F. H. Schacher, B. Wang, D. E. Demco, A. Walther, *Nat. Commun.* **2015**, *6*, 5967.

© 2018 WILEY-VCH Verlag GmbH & Co. KGaA, Weinheim